RSC Advances

PAPER

View Article Online
View Journal | View Issue

Check for updates

Cite this: *RSC Adv.*, 2022, **12**, 33501

Robust acid–base Ln-MOFs: searching for efficient catalysts in cycloaddition of CO_2 with epoxides and cascade deacetalization–Knoevenagel reactions†

Xuezhen Si,[a] Xuze Pan,[a] Jintang Xue,[a] Qingxia Yao, *[a] Xianqiang Huang, [a] Wenzeng Duan, [a] Yi Qiu,*[b] Jie Su,[b] Minglei Cao[c] and Jun Li*[a]

Received 17th October 2022
Accepted 17th November 2022

DOI: 10.1039/d2ra06545b

rsc.li/rsc-advances

A family of microporous and robust Ln(III)-based metal–organic frameworks (**1-Ln**, Ln = Sm, Eu, Gd, Tb, Dy, Ho, Er, Yb) have been obtained using 4,4′,4″-nitrilotribenzoic acid (H_3NTB) in NMP–HCl solvent. Both single-crystal and powder X-ray diffraction analyses demonstrate that **1-Ln** are isostructural and possess 3D frameworks with permanent porosity for Ar and CO_2 adsorption. Strikingly, the incorporation of both Lewis acidic lanthanide ions and the basic triphenylamine group into **1-Ln** makes them efficient acid–base catalysts for both cycloaddition of epoxides with CO_2 and one-pot cascade deacetalization–Knoevenagel reactions. The systematic catalytic studies show that **1-Tb** and **1-Yb** possess the best catalytic activities for both reactions, indicating the catalytic activities of these Ln-MOFs are strongly dependent on metal Lewis acid sites embedded in the frameworks.

Introduction

Recently, lanthanide based metal–organic frameworks (Ln-MOFs) have been intensely investigated as heterogeneous catalysts because of their unique features, such as inherent porosity, tunable pore sizes, reusability, and a broad range of catalytic sites.[1–3] In principle, the active sites of Ln-MOF catalysts can be (i) lanthanide ions with unsaturated coordination environments, (ii) organic or organometallic functional sites realized using pre-designed ligands, and (iii) other catalytic species encapsulated in the pores. The integration of these catalytic sites into one material would promise the Ln-MOFs a powerful platform for heterogeneous catalysis. Currently, Ln-MOFs as Lewis acids have been applied for a number of organic transformations, including cycloaddition of CO_2, Knoevenagel condensation, and Heck reactions.[4–6]

Carbon dioxide (CO_2), as the primary greenhouse gas, is also a nontoxic, economic, and renewable C1 building block. CO_2 capture and conversion into value-added chemicals are attractive in terms of green chemistry.[7,8] Particularly, the cycloaddition of epoxides and CO_2 into cyclic carbonates is considered to be one of the most promising approaches for CO_2 utilization, given the wide industrial applications of the target cyclic carbonates.[9,10] In recent years, it has been reported that some porous Ln-MOFs have shown preeminent catalytic performances on cycloaddition reactions of epoxides and CO_2, mainly because these MOFs feature selective CO_2 capture and lanthanide ions as Lewis acid sites to activate epoxide.[11–15]

On the other hand, among various catalytic processes, cascade reactions are sequentially proceeded with two or multiple transformations in one-pot, which eliminate the time-consuming isolation and purification of intermediates.[16–18] However, some cascade reactions require the catalysts with antagonistic catalytic sites (*e.g.*, Lewis acidic sites for the first step and basic sites for the second step in deacetalization–Knoevenagel reaction or deacetalization–Henry reaction). Therefore, the catalyst design toward these one-pot cascade reactions is challenging.[19–23] In this respect, Ln-MOFs offer the unique possibility of combining isolated Lewis acidic and basic active sites for cascade or cooperative catalysis. To date, several acid–base bifunctional MOFs have shown to be high-performance catalysts for one-pot cascade reactions.[4,11,24–26]

The Knoevenagel reaction as one important synthetic method for the C–C bond formation, is typically catalyzed by base,[27] and triphenylamine groups in a MOF as a weak base for the Knoevenagel reaction have been reported by Duan's and Wen's group.[28,29] Meanwhile, the lanthanide ions embedded in Ln-MOFs have proven to be valuable Lewis acid sites for a number of organic reactions, as mentioned before.[4–6] Bearing these considerations in mind, one would expect a Ln-MOF incorporating triphenylamine group to be an acid–base

[a]School of Chemistry and Chemical Engineering and Shandong Provincial Key Laboratory/Collaborative Innovation Center of Chemical Energy Storage and Novel Cell TechnologyLiaocheng University, Liaocheng 252000, China. E-mail: yaoqxlcu@163.com; Junli@lcu.edu.cn

[b]College of Chemistry and Molecular Engineering, Peking University, Beijing, 100871, PR China. E-mail: qiuyi@pku.edu.cn

[c]Shandong Ruijie New Material Co., Ltd, Liaocheng 252000, China

† Electronic supplementary information (ESI) available. CCDC 2210635 and 2210636. For ESI and crystallographic data in CIF or other electronic format see DOI: https://doi.org/10.1039/d2ra06545b

bifunctional catalyst for both cycloaddition of epoxides with CO_2 and one-pot deacetalization–Knoevenagel reaction.

In this work, using 4,4′,4″-nitrilotribenzoic acid (H_3NTB, a typical triphenylamine ligand) and lanthanide nitrates dissolved in NMP–HCl mixture, we have solvothermally synthesized a new family of 3D microporous Ln-MOFs (denoted **1-Ln**, Ln = Sm, Eu, Gd, Tb, Dy, Ho, Er, Yb). The structural analyses reveal **1-Ln** are intrinsically isostructural, which offer the opportunity to determine the effect of the metal center on catalytic performance. All **1-Ln** solids exhibit remarkable robustness and permanent porosity evaluated by Ar adsorption analysis. Their CO_2 adsorption at 273, 298 K/1 bar are also investigated. Interestingly, the incorporation of both Lewis acidic lanthanide ions and basic triphenylamine group into one single framework makes them highly efficient catalysts for both cycloaddition of epoxides with CO_2 and one-pot cascade deacetalization–Knoevenagel condensation reactions. Among them, **1-Tb** and **1-Yb** possess the best catalytic activities for both two reactions. More strikingly, the systematic catalytic studies reveal that the catalytic activities of these Ln-MOFs are strongly dependent on Lewis acidic lanthanide ions embedded in the framework, uncovering the possibilities to develop Tb- and Yb-MOFs as high-performance Lewis acid catalysts.

Results and discussion

Structure analyses of 1-Ln crystals

Solvothermal reactions of different lanthanide salts with H_3NTB in NMP–HCl mixture harvest a family of crystalline Ln-MOFs, **1-Ln** (Ln = Sm, Eu, Gd, Tb, Dy, Ho, Er, Yb), which are isostructural as checked by powder X-ray diffraction (XRD, Fig. 2) and infrared spectroscopy (Fig. S3†). Under the same synthetic conditions, $LaCl_3\cdot 6H_2O$ affords a different structure that would be reported in due course. Single crystal X-ray diffraction (SCXRD) analyses of **1-Tb** and **1-Yb** show that they crystallize in the triclinic space group $P\bar{1}$ (Table S1†) and have the formula of $\{[Ln(NTB)(NMP)]\cdot(NMP)\}_n$, which are in good accordance with their TG analyses (Fig. S4†). SCXRD analyses reveal **1-Ln** have a porous architecture (Fig. 1 and 2). Therefore, only the structure of **1-Yb** is briefly discussed herein. The asymmetric unit of **1-Yb** contains one Yb^{3+} cation, one NTB^{3-} ligand, one coordinated and one free guest NMP molecule (Fig. S1†). As shown in Fig. 1a, each Yb^{3+} is coordinated by seven oxygen atoms from one NMP molecule and six μ_2-η^1:η^1 carboxylate groups that belong to six different ligands. Interestingly, every two Yb^{3+} ions are four-fold bridged by four μ_2-η^1:η^1 carboxylate groups to form a dimeric unit. These dimeric units are further two-fold bridged by another two μ_2-η^1:η^1 carboxylate groups to generate a 1D Yb-COO inorganic chains running along [100] (Fig. 1b). These Yb-COO inorganic chains are connected by NTB^{3-} ligands to define the three-dimensional porous framework (Fig. 2). The framework possesses two kinds of rhombus channels, one with diagonals of 7.1 × 5.9 $Å^2$ (measured between the opposite atoms of N⋯N and Yb⋯Yb, and considering the van der Waals radii) along [100] which are aligned by coordinated NMP molecules, and the other one with diagonals of 8.8 × 5.8 $Å^2$ (measured between the opposite atoms of N⋯N and

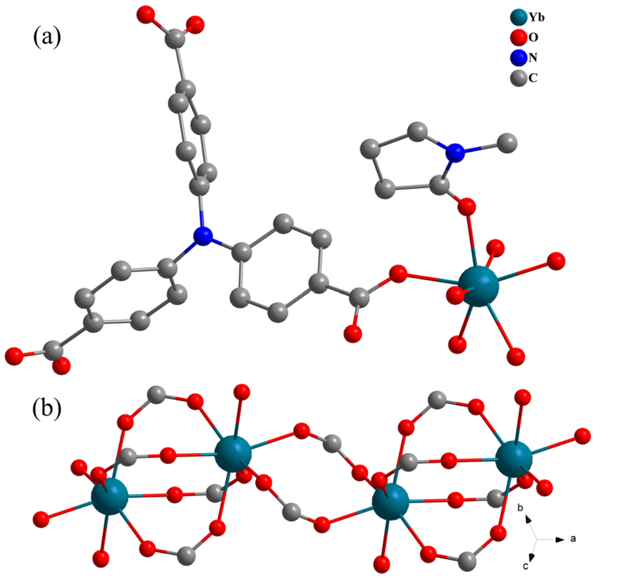

Fig. 1 (a) The coordination environment around Yb^{3+} in the **1-Yb**; (b) 1D Yb-COO inorganic chain.

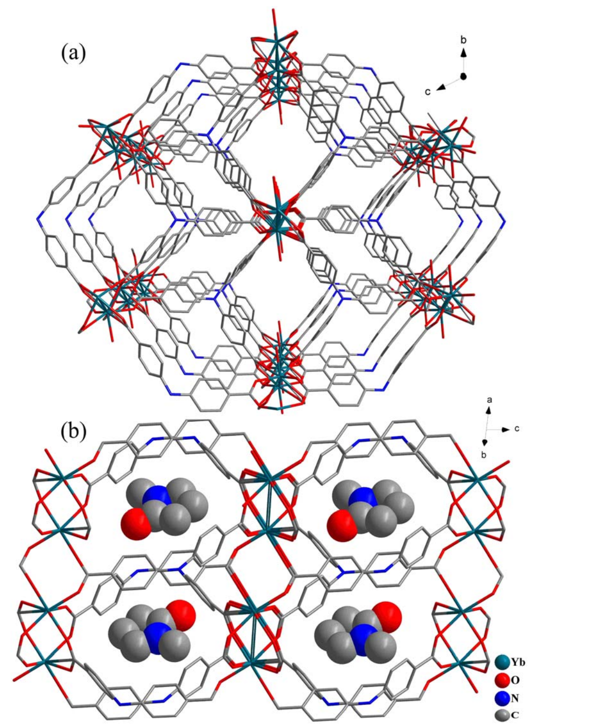

Fig. 2 (a) 3D porous framework of **1-Yb** showing channels along [100], with removal of all coordinated and guest NMP molecules for clarity; (b) perspective view of channels along [110], with NMP guest molecules occupying the channels.

Yb⋯Yb) along [110] which are filled by guest NMP molecules. After removal of all NMP molecules, the free void calculated by PLATON is up to 47.4% of the crystal volume. Thus, **1-Yb** is a highly microporous framework, which would be suitable for gas adsorption. Moreover, the incorporation of Lewis acidic lanthanide centers and Lewis basic triphenylamine sites in the channels indicates that **1-Yb** could be a potential acid–base heterogeneous catalyst. With these structures (**1-Sm**, Eu, Gd, Tb, Dy, Ho, Er, Yb) in hand, comparative experiments were performed to determine the effect of the metal centers on catalytic performance and to search for more efficient catalysts.

PXRD analyses, thermal stability of the frameworks, Ar and CO_2 adsorption isotherms

The PXRD profiles of as-synthesized **1-Ln** solids match well with their simulated ones, verifying the phase purity of the as-synthesized bulk samples (Fig. S2†). Furthermore, all **1-Ln** solids display similar and excellent thermal stability (Fig. S4†). As shown by thermogravimetric analyzer (TGA), the guest-free phases of **1-Ln** are thermally stable up to 500 °C. This exceptional robustness of the frameworks is also observed in other Ln-MOFs structurally built on Ln-COO inorganic chains.[30–33]

Ar adsorption experiments were performed at 87 K to assess the permanent porosity of all compounds. The adsorption isotherms (Fig. 3 and S5†) demonstrate type-I adsorption which is typical of microporous materials, with the BET (Brunauer–Emmett–Teller) surface area of 113.7 (**1-Sm**), 128.1 (**1-Eu**), 222.0 (**1-Gd**), 299.0 (**1-Tb**), 268.8 (**1-Dy**), 261.2 (**1-Ho**), 274.7 (**1-Er**), and 300.7 (**1-Yb**) $m^2\ g^{-1}$, respectively. The total pore volumes are 0.105 (**1-Sm**), 0.111 (**1-Eu**), 0.152 (**1-Gd**), 0.204 (**1-Tb**), 0.176 (**2-Dy**), 0.182 (**1-Ho**), 0.202 (**1-Er**), and 0.209 (**1-Yb**) $cm^3\ g^{-1}$, respectively. These values are comparable to other porous lanthanide MOFs.[33–35]

Encouraged by the robustness and permanent porosity of **1-Ln**, we investigated their CO_2 adsorption behaviors. It is clearly demonstrated that all **1-Ln** solids are readily accessible to CO_2 (Fig. S5†). For **1-Tb** and **1-Yb**, their CO_2 adsorption isotherms at 273 and 298 K are shown in Fig. 3. The maximal CO_2 capacities is 27.5, 15.9 $cm^3\ g^{-1}$ (for **1-Tb**) and 29.4, 16.5 $cm^3\ g^{-1}$ (for **1-Yb**) respectively. In order to gain more insights into the framework–CO_2 interactions, adsorption heat of CO_2 (Q_{st}) was calculated by using the viral equation based on the isotherms at 273 K and 298 K. As shown in Fig. S6,† the Q_{st} value at zero coverage is around 22.5 kJ mol^{-1} (for **1-Tb**) and 25.0 kJ mol^{-1} (for **1-Yb**), respectively, which are comparable to some MOFs such as $[Zn_2(L)(dpe)_2](NO_3)\cdot(DMF)_3\cdot(H_2O)_2$ (20.5 kJ mol^{-1}; L = 1,3-bis(3,5-dicarboxyphenyl)imidazolium, dpe = 1,2-di(4-pyridyl) ethylene)[36] and FJU-14-BF_4 (18.8 kJ mol^{-1}),[37] indicating moderate interactions between the framework and guest CO_2 molecules.

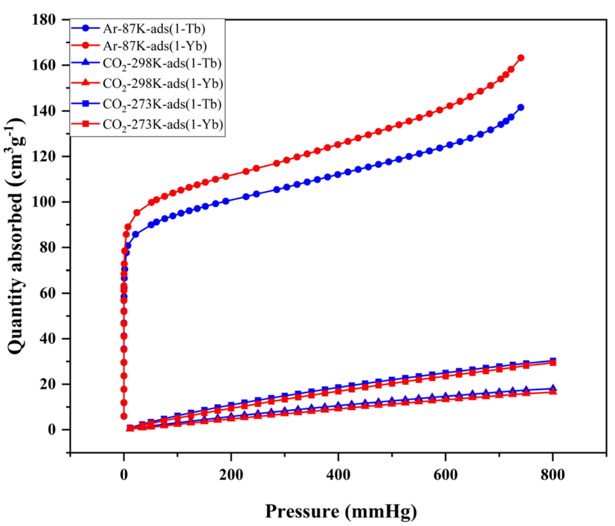

Fig. 3 The Ar adsorption isotherms at 87 K and the CO_2 adsorption isotherms at 273 K and 298 K of **1-Tb** and **1-Yb**.

Catalytic cycloaddition of CO_2 and epoxides

On account of the considerable CO_2 adsorption quantity, the accessible channels, and the coexisting Lewis acid–base sites, the catalytic performances of **1-Ln** towards the cycloaddition of CO_2 and epoxides into cyclic carbonates are investigated. We wonder the effect of the metal center on catalytic performance among the eight Ln-MOF candidates (**1-Sm**, Eu, Gd, Tb, Dy, Ho, Er, Yb). Firstly, with **1-Yb** and *n*-Bu_4NBr (tetra-*n*-tertbutylammonium bromide) as catalytic system, the cycloaddition between CO_2 and epichlorohydrin under ambient temperature has been used as a model reaction to screen the optimal conditions. After detailed investigations, the optimal conditions are set as follows: epichlorohydrin (4 mmol), CO_2 (1 atm), **1-Yb** catalyst (0.02 mmol based on Ln metal sites; 0.5 mol%) and cocatalyst *n*-Bu_4NBr (0.2 mmol; 5 mol%), room temperature, 36 hours. As seen in Table 1, in the case of the reaction without any catalyst (entry 1), the reaction does not proceed. Without

Table 1 Cycloaddition of CO_2 and epichlorohydrin with different **1-Ln** catalysts[a]

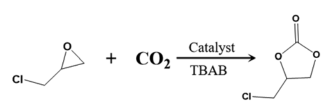

Entry	Catalyst	Catalyst (mol%)	*n*-Bu_4NBr (mol%)	Yield[b] (%)
1	—	0	0	<1.0
2	**1-Yb**	0.5	0	12.0
3	—	0	5	4.8
4	**1-Yb**	0.5	5	97.0
5	**1-Sm**	0.5	5	89.0
6	**1-Eu**	0.5	5	83.0
7	**1-Gd**	0.5	5	95.0
8	**1-Tb**	0.5	5	99.0
8	**1-Dy**	0.5	5	79.0
9	**1-Ho**	0.5	5	81.0
10	**1-Er**	0.5	5	87.0

[a] Reaction conditions: 4 mmol of epichlorohydrin, solvent free, CO_2 (1 atm). [b] The yields were determined by ^1H NMR spectrum of the crude reaction mixtures.

cocatalyst *n*-Bu_4NBr, pure **1-Yb** catalyst shows a low conversion of 12.0% (entry 2); while without **1-Yb**, *n*-Bu_4NBr alone lead to almost no reactivity (4.8%, entry 3). However, when **1-Yb** catalyst and cocatalyst *n*-Bu_4NBr were added as a binary catalytic system (entry 4), the conversion of epichlorohydrin is up to 97%, highlighting the remarkable synergistic effect of the binary catalytic system.

Then using the optimized conditions, we extend this reaction to other seven isomorphic MOF candidates to search for efficient catalysts and determine the effect of the metal centers on catalytic performances. As illustrated in Table 1, the comparative catalytic results reveal that **1-Ln** solids are all valuable catalyst candidates for cycloaddition reaction of CO_2 and epoxides. Among them, **1-Gd**, Tb and Yb demonstrate the highest catalytic activity, comparable to the most effective MOF catalysts reported in literature (see Table S3†). Fig. 4 demonstrates the relationship between the catalytic yield of each Ln-MOFs and atomic number of Ln (Z_{Ln}). It is found that the catalytic yield shows two increase stages, one with a gradual increase from Sm (89%) to Tb (99%) and then an abrupt decrease at Dy (79%), and the other one with gradual increase from Dy to Yb (97%).

Generally, the strength of a Lewis acid is a critical factor in determining its catalytic activity, because a certain threshold of Lewis acidity is required to induce catalytic chemical transformations. In Fig. 4, we also plot the empirical scale for Lewis acid strength of Ln^{3+} along with Z_{Ln} based on the reported data, showing an almost linear increase of Lewis acid strength of Ln^{3+} against Z_{Ln}; the heavier Ln^{3+}, the more Lewis acidic.[38] Obviously, the trend of the catalytic yield (activity) of Ln-MOFs *vs.* Z_{Ln} does not coincide with that of the Lewis acid strength *vs.* Z_{Ln}. These analyses demonstrate that the catalytic activity of Ln-MOFs, at least for **1-Tb**, is not solely dependent on Lewis acid strength of Ln^{3+}, but also on some other factors. We tend to presume that, compared to Yb^{3+}, the lighter lanthanide ions like Tb^{3+} possesses high and variable coordination number allowing easy rearrangements for substrate activation.[39,40] Therefore, we attribute the anomalously high activity of **1-Tb** to the combining effect of the modest Lewis acid strength and the labile coordination environment of Tb^{3+} during the catalysis. Note that the underlying mechanic path of **1-Tb** and **1-Yb** may be different, and new systems or experiments should be designed to elucidate the exact catalytic mechanism in the future. Importantly, the present study not only confirms the available Lewis acidity of Ln^{3+} ions in MOFs, but also point out the way to develop Tb- and Yb-MOFs as high-performance Lewis acid catalysts.

Lastly, with the optimal catalysts in hand, we turn our attention to the recyclability, stability, and catalytic generality of **1-Yb** as a heterogeneous catalyst. **1-Yb** can be readily recovered, washed thoroughly with CH_2Cl_2, and used for next runs. Within five catalytic runs, high yields of 97–99% are maintained (Fig. S7†), suggesting that **1-Yb** possessed high recyclability to the cycloaddition reaction. In addition, a PXRD pattern of **1-Yb** recovered from the fifth run is consistent with the one of the as-synthesized, confirming the structural integrity of **1-Yb** during the catalytic process (Fig. S8†). Furthermore, the catalytic generality over **1-Yb** can be extended to several typical epoxide substrates with product yields from moderate to good (Table S2†). These results show that stability and heterogeneous nature of the **1-Yb** catalyst. Based on structural analysis and catalytic performances of **1-Yb**, a tentative synergistic catalytic mechanism for the cycloaddition of CO_2 and epoxides over **1-Yb**/*n*-Bu_4NBr is proposed in Fig. S9.† First, dissociation of coordinated NMP of **1-Yb** occurs and the open Lewis Yb active site coordinates with oxygen atom of the epoxide. This coordination bond polarizes the C–O bond to activate the epoxide. The activated epoxide is opened by Br^- ion of TBAB to generate a metal-ordinated bromoalkoxide intermediate. Next, CO_2 was nucleophilically attacked by the O atom of bromoalkoxide to form a metal carbonate, which is finally converted to cyclic carbonate by intramolecular (SN_2-type nucleophilic) ring-closure reaction, regenerating the catalyst and co-catalyst.[10]

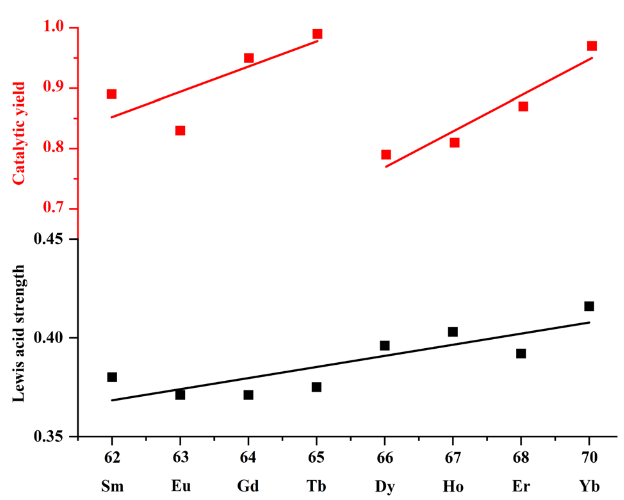

Fig. 4 The trend chart showing catalytic yield (activity) of Ln-MOFs *vs.* Z_{Ln} in catalyzing CO_2-cycloaddition reaction and the Lewis acid strength of Ln^{3+} *vs.* Z_{Ln}.

Catalytic deacetalization–Knoevenagel reactions

Owing to the incorporation of both lanthanide Lewis acidic sites and triphenylamine Lewis basic sites within their porous frameworks, **1-Ln** could be viewed as a kind of potential bifunctional acid–base catalysts. In order to prove this point, **1-Ln** crystals were used to study their catalytic activities on one-pot cascade deacetalization–Knoevenagel reactions. The reaction between benzaldehyde dimethylacetal (BD) and malononitrile (MA) under solvent-free condition was taken as the template reaction to investigate the catalytic activities of these Ln-MOF solids (Table 2). At the first step of the catalysis, Ln ions as a Lewis acid can catalyze the deprotection of BD to give benzaldehyde (BA), and at the second step, triphenylamine as a weak Lewis base can catalyze Knoevenagel condensation reaction between BA and MA to afford benzylidene malononitrile (BM).

Table 2 One-pot cascade deacetalization–Knoevenagel reaction between benzaldehyde dimethylacetal (BD) and malononitrile (MA) catalyzed by different **1-Ln** catalysts[a]

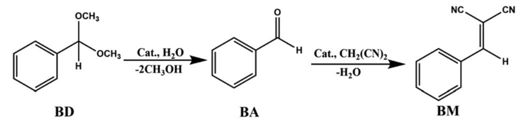

Entry	Catalyst	Conversion of BD[b] (%)	Conversion of BA[c] (%)	Yield of BM[b] (%)
1[d]	**1-Yb**	0	0	0
2[e]	—	0	0	0
3	**1-Sm**	83	81	68
4	**1-Eu**	93	83	78
5	**1-Gd**	96	96	93
6	**1-Tb**	98	100	98
7	**1-Dy**	79	98	77
8	**1-Ho**	88	96	84
9	**1-Er**	86	97	86
10	**1-Yb**	97	100	97

[a] Reaction conditions: BD (1 mmol), H_2O (3 mmol), MA (2 mmol), catalysts (0.5 mol%), 60 °C, 6 h, N_2 atmosphere. [b] The yields were determined by ^1H NMR spectrum of the crude reaction mixtures. [c] The conversion of intermediate BA is defined by the ratio of (yield of BM)/(conversion of BD). [d] Control experiment was performed without water in the presence of **1-Yb**. [e] Control experiment was done without **1-Yb** in the presence of water.

The catalytic reactions were performed using the following conditions: BD (1 mmol), H_2O (3 mmol), MA (2 mmol), catalysts (0.5 mol%), 60 °C, 6 h, N_2 atmosphere. Experimental results are given in Table 2, showing that **1-Ln** solids are all valuable catalyst candidates for one-pot cascade reaction. Among them, **1-Tb** and **1-Yb** demonstrate the highest catalytic activity. Control experiments were also performed to figure out the role of components during the catalytic procedure. H_2O was necessary in the deacetalization (step I) process, as the reaction was sluggish without water even in the presence of **1-Yb** (entry 1). As shown in entry 2, the reaction did not proceed without **1-Yb**.

In order to clarify the active catalytic site for each step, we calculate and plot the conversion of BD and intermediate BA, and the yield of BM against Z_{Ln} (the coordination number of Ln) in Table 2 and Fig. 5. The conversion of BD to BA in first step (Fig. 5a) clearly show that all Ln^{3+} cations in MOFs have the Lewis acidity enough to efficiently catalyze the deprotection of BD, with two maxima at **1-Tb** (98%), **1-Yb** (97%) and two minima at **1-Sm** (83%) and **1-Dy** (79%). At the first step of the one-pot catalysis, the trend of the catalytic activity in Ln-MOFs is not regularly increased along with Z_{Ln} but very similar to that found in catalytic cycloaddition of CO_2 and epoxides, demonstrating Ln^{3+} cations embedded in MOF as Lewis acids is distinct from homogeneous species, possible due to their unique coordination environment in MOF solid. In second step, the conversion of intermediate BA to the product BM, which is defined by the ratio of (yield of BM)/(conversion of BD), is increased from 81% for Sm to almost 100% for Gd, Tb, Dy, Ho, Er, Yb (Fig. 5b). Generally, Knoevenagel condensation reactions are considered to be base-catalyzed.[27–29] However, for comparison, control experiments show that the conversion of BA to BM catalyzed by sole triphenylamine or H_3NTB is only 70 or 46%, respectively. The present study confirms that Ln^{3+} especially for Tb^{3+}, Yb^{3+} in MOFs plays an important role in accelerating the Knoevenagel reaction. This synergistic effect of the Lewis acidic metal centers and Lewis base sites in porous MOFs on catalyzing Knoevenagel reaction is also observed in other scientific studies.[6,29,31,41]

The above analyses reveal that both steps are strongly correlating with the catalytic activity of lanthanide ions embedded in the framework. As a consequence, the total yields of BM show **2-Tb** and **2-Yb** have the highest catalytic activity towards one-pot reaction. Interestingly, similar to that found in Fig. 4, the trend of catalytic activity of each Ln-MOFs *vs.* Z_{Ln}

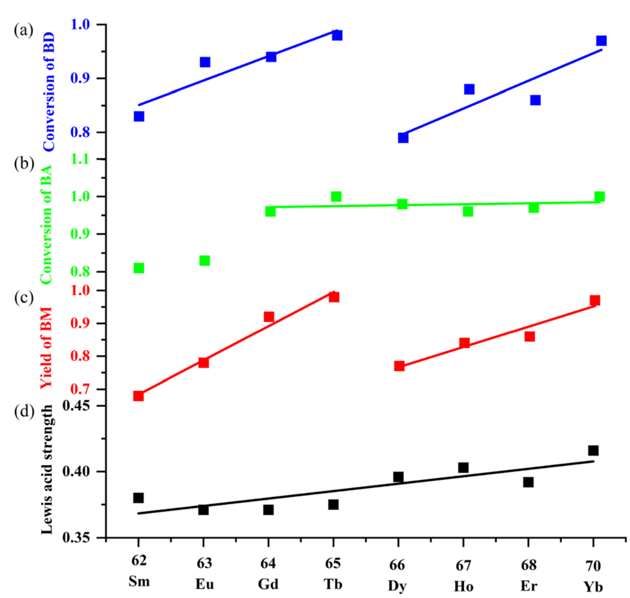

Fig. 5 The trend chart showing (a) the conversion of BD, (b) the conversion of intermediate BA, and (c) the yield of BM *vs.* Z_{Ln} (the coordination number of Ln) in catalyzing one-pot cascade reaction and (d) the Lewis acid strength of Ln^{3+} *vs.* Z_{Ln}.

(Fig. 5c) also shows two increase stages, one with a gradual increase from Sm (68%) to Tb (98%) and then an abrupt decrease at Dy (77%), and the other one with gradual increase from Dy (77%) to Yb (97%). Once again, the present study confirm the feasibility to develop Tb- and Yb-MOFs as high-performance Lewis acid catalysts, comparable to the most effective MOF catalysts reported in literature (see Table S5†).

Finally, we investigate the recyclability, stability, and catalytic generality of **1-Yb**. After five consecutive catalytic runs under optimized conditions, **1-Yb** kept high catalytic activity (Fig. S10†). Moreover, the PXRD patterns between the recovered and the original one are almost identical, confirming the structural integrity of **1-Yb** (Fig. S11†). The recovered **1-Yb** was also evaluated by Ar adsorption, showing the retention of the porous framework (Fig. S12†). In addition, **1-Yb** had the general high catalytic activity on a series of epoxides with various substitutes under the optimal reaction conditions (Table S4†). All results show the stability and heterogeneous nature of the **1-Yb** catalyst. Based on the structure and catalytic behaviors of **1-Yb**, a possible catalytic mechanism for one-pot cascade deacetalization–Knoevenagel reaction on **1-Yb** is proposed in Fig. S13.†

Conclusions

In summary, we have synthesized a family of robust and microporous Ln-MOFs (**1-Ln**, Ln = Sm, Eu, Gd, Tb, Dy, Ho, Er, Yb) based on H_3NTB, demonstrating permanent porosity for Ar and CO_2 adsorption abilities. Importantly, the combination of Lewis acidic lanthanide ions and basic triphenylamine group into the framework of **1-Ln** makes them efficient acid–base catalysts for both cycloaddition of CO_2 with epoxides and one-pot cascade deacetalization–Knoevenagel reactions. Among them, **1-Tb** and **1-Yb** demonstrates the best catalytic activities for both two reactions. More strikingly, the systematic catalytic studies reveal that the catalytic activities of these Ln-MOFs are strongly dependent on Lewis acidic lanthanide ions embedded in the framework, opening up the possibilities to develop Tb- and Yb-MOFs as high-performance Lewis acid catalysts. Work is underway to synthesize new Ln-MOFs in our lab.

Experimental

Materials and instruments

Materials and instruments can be seen in ESI S1† part.

Synthesis

Synthesis of {[Sm(NTB)(NMP)]·(NMP)}$_n$ (1-Sm). A mixture of $Sm(NO_3)_3\cdot6H_2O$ (16.0 mg), H_3NTB (23.3 mg), NMP (1.0 mL), HCl (0.01 M, 0.2 mL), H_2O (0.3 mL) was sealed in a 23.0 mL Teflon-lined stainless-steel container, which was heated at 85 °C for 21 hours to afford block crystals. The collected crystals were dried in air at room temperature. Yield: 11.24 mg. IR/cm^{-1} (KBr): 3424 (br), 3045 (w), 2925 (w), 2873 (w), 1687 (m), 1627 (m), 1584 (m), 1534 (m), 1393 (m), 1332 (m), 1178 (m), 1144 (w), 1117 (w), 1015 (w), 925 (w), 831 (m), 783 (s), 719 (m), 659 (w), 628 (w), 580 (m), 529 (w), 506 (m), 470 (w), 441 (w).

Synthesis of {[Eu(NTB)(NMP)]·(NMP)}$_n$ (1-Eu). 1-Eu was synthesized by using the same procedure except by using $Eu(NO_3)_3\cdot6H_2O$ (16.6 mg). Yield: 9.51 mg. IR/cm^{-1} (KBr): 3430 (br), 3044 (w), 2926 (w), 2873 (w), 1687 (m), 1628 (m), 1585 (m), 1535 (m), 1392 (s), 1332 (m), 1262 (w), 1177 (m), 1144 (w), 1015 (w), 831 (m), 784 (s), 719 (m), 659 (w), 628 (w), 559 (m), 529 (w), 506 (m), 470 (w), 441 (w).

Synthesis of {[Gd(NTB)(NMP)]·(NMP)}$_n$ (1-Gd). 1-Gd was synthesized by using the same procedure except by using $Gd(NO_3)_3\cdot6H_2O$ (14.5 mg). Yield: 11.49 mg. IR/cm^{-1} (KBr): 3393 (br), 2926 (w), 1686 (w), 1655 (w), 1625 (w), 1585 (w), 1535 (w), 1401 (s), 1315 (w), 1275 (w), 1170 (m), 1106 (w), 1014 (w), 924 (m), 582 (m), 784 (s), 710 (m), 659 (w), 628 (w), 565 (m), 525 (w), 505 (m), 470 (w), 442 (w).

Synthesis of {[Tb(NTB)(NMP)]·(NMP)}$_n$ (1-Tb). 1-Tb was synthesized by using the same procedure except by using $Tb(NO_3)_3\cdot6H_2O$ (27.2 mg). Yield: 25.65 mg. IR/cm^{-1} (KBr): 3319 (br), 1654 (m), 1596 (m), 1532 (m), 1401 (s), 1316 (w), 1281 (w), 1176 (m), 1150 (w), 1105 (w), 1013 (m), 954 (m), 859 (m), 783 (s), 710 (m), 672 (w), 628 (w), 568 (m), 521 (w),496 (w), 438 (w).

Synthesis of {[Dy(NTB)(NMP)]·(NMP)}$_n$ (1-Dy). 1-Dy was synthesized by using the same procedure except by using $Dy(NO_3)_3\cdot6H_2O$ (18.3 mg). Yield: 19.97 mg. IR/cm^{-1} (KBr): 3434 (br), 3044 (w), 2916 (w), 2873 (w), 1687 (m), 1630 (m), 1585 (m), 1537 (w), 1393 (s), 1331 (w), 1307 (w), 1260 (w), 1178 (w), 1144 (w), 1116 (w), 1015 (w), 865 (w), 831 (w), 783 (s), 719 (w), 659 (w), 628 (w), 584 (w), 561 (w), 530 (w), 506 (w), 470 (w), 442 (w).

Synthesis of {[Ho(NTB)(NMP)]·(NMP)}$_n$ (1-Ho). 1-Ho was synthesized by using the same procedure except by using $Ho(NO_3)_3\cdot6H_2O$ (17.6 mg). Yield: 20.51 mg. IR/cm^{-1} (KBr): 3428 (br), 3044 (w), 2925 (w), 2874 (w), 1687 (m), 1632 (m), 1586 (m), 1539 (m), 1514 (w), 1401 (s), 1331 (m), 1261 (w), 1178 (w), 1145 (w), 1117 (w), 1105 (w), 866 (w), 832 (m), 784 (s), 719 (m), 659 (m), 628 (w), 585 (m), 563 (w), 531 (w), 507 (w), 470 (w), 443 (w).

Synthesis of {[Er(NTB)(NMP)]·(NMP) }$_n$ (1-Er). 1-Er was synthesized by using the same procedure except by using $Er(NO_3)_3\cdot6H_2O$ (30.0 mg). Yield: 21.32 mg. IR/cm^{-1} (KBr): 3424 (br), 3044 (w), 2919 (w), 2873 (w), 1687 (m), 1632 (m), 1586 (m), 1539 (m), 1512 (w), 1401 (s), 1307 (m), 1261 (w), 1178 (w), 1145 (w), 1117 (w), 1015 (w), 866 (w), 832 (m), 784 (s), 719 (m), 659 (m), 627 (w), 585 (m), 563 (w), 531 (w), 507 (w), 470 (w), 442 (w).

Synthesis of {[Yb(NTB)(NMP)]·(NMP)}$_n$ (1-Yb). 1-Yb was synthesized by using the same procedure except by using $YbCl_3\cdot6H_2O$ (15.5 mg). Yield: 9.62 mg. IR/cm^{-1} (KBr): 3415 (br), 3044 (w), 2921 (w), 2874 (w), 1687 (m), 1633 (m), 1588 (m), 1540 (m), 1512 (w), 1401 (s), 1331 (m), 1261 (w), 1178 (w), 1145 (w), 1117 (w), 1105 (w), 925 (w), 866 (w), 833 (w), 784 (s), 719 (m), 659 (m), 628 (w), 588 (m), 565 (w), 531 (w), 509 (w), 471 (w), 443 (w).

Single-crystal structure characterization of the 1-Ln crystals

SCXRD data for **1-Tb** and **1-Yb** were performed on a Rigaku Oxford X-ray Diffractometer with graphite-monochromated MoKα radiation (λ = 0.71073 Å) at 293 K. All absorption corrections were applied using multi-scan technique. The crystal structures of **1-Ln** were solved by the direct method and refined through full-matrix least-squares techniques method on F^2 using the Olex2 crystallographic software package.[42,43] Full crystallographic data for **1-Tb** and **1-Yb** has been deposited with the CCDC 2210635 and 2210636. The crystallographic data for **1-Tb** and **1-Yb** are summarized in Table S1.†

Ar and CO_2 adsorption isotherms

Ar adsorption isotherm was recorded at 87 K on a micromeritics ASAP2460 analyzer. The sample was activated under vacuum by heating at 200 °C overnight. The specific surface area was calculated from the data in the adsorption branch at p/p_0 = 0.05–0.30. The total pore volume was calculated from the uptake at p/p_0 of 0.950. CO_2 adsorption isotherms was performed at 273 and 298 K respectively.

General procedure for cycloaddition of CO_2 and epoxides

In a typical catalytic reaction, epichlorohydrin (4 mmol) and cocatalyst n-Bu_4NBr (0.2 mol; 5 mol%) were added to the Schlenk tube, to which was further added **1-Ln** (Ln = Sm, Eu, Gd, Tb, Dy, Ho, Er, Yb) (2 mol% based on metal ion), and then slowly stirred under 1 atm CO_2 pressure for 36 hours at room temperature.

General procedure for one-pot cascade deacetalization–Knoevenagel reactions

In a typical catalytic reaction, benzaldehyde dimethylacetal (1 mmol), H_2O (3 mmol) and malononitrile (2 mmol) and were added to the Schlenk tube, to which was further added **1-Ln** (Ln = Sm, Eu, Gd, Tb, Dy, Ho, Er, Yb) (2 mol% based on Ln^{3+}), and then slowly stirred for 6 hours at 60 °C in a nitrogen atmosphere.

Author contributions

Qingxia Yao, Yi Qiu, Jun Li: project administration, supervision. Xuezhen Si, Qingxia Yao: writing original draft, methodology, data collection and analysis. Xuze Pan, Jintang Xue, Minglei Cao, Wenzeng Duan, Xianqiang Huang: data collection and analysis. Yi Qiu, Jie Su: X-ray single-crystal structural analysis.

Conflicts of interest

There are no conflicts to declare.

Acknowledgements

The work was financially supported by the Natural Science Foundation of Shandong Province (No. ZR2022MB137 and ZR2019MB043), the National Natural Science Foundation of China (22003003, 21871125, and 21501086). Yao Q. thanks the financial supports from Liaocheng University (319260119, HFC202119) and the Scientific Research Foundation for the Returned Overseas Chinese Scholars, State Education Ministry.

Notes and references

1 Ć. Pagis, M. Ferbinteanu, G. Rothenberg and S. Tanase, Lanthanide-based metal organic frameworks: synthetic strategies and catalytic applications, *ACS Catal.*, 2016, **6**(9), 6063–6072.
2 X. Shi, B. Cao, J. Liu, J. Zhang and Y. Du, Rare-earth-based metal–organic frameworks as multifunctional platforms for catalytic conversion, *Small*, 2021, **17**, 2005371.
3 Y. Zhang, S. Liu, Z.-S. Zhao, Z. Wang, R. Zhang, L. Li and Z.-B. Han, Recent progress in lanthanide metal–organic frameworks and their derivatives in catalytic applications, *Inorg. Chem. Front.*, 2021, **8**, 590–619.
4 H. Chen, S. Liu, H. Lv, Q.-P. Qin and X. Zhang, Nanoporous $\{Y_2\}$–organic frameworks for excellent catalytic performance on the cycloaddition reaction of epoxides with CO_2 and deacetalization–Knoevenagel condensation, *ACS Appl. Mater. Interfaces*, 2022, **14**, 18589–18599.
5 G.-Q. Huang, J. Chen, Y.-L. Huang, K. Wu, D. Luo, J. K. Jin, J. Zheng, S.-H. Xu and W. Lu, Mixed-linker isoreticular Zn(II) metal–organic frameworks as brønsted acid–base bifunctional catalysts for Knoevenagel condensation reactions, *Inorg. Chem.*, 2022, **61**, 8339–8348.
6 T. Zhang, H. Chen, S. Liu, H. Lv, X. Zhang and Q. Li, Highly Robust $\{Ln_4\}$–organic frameworks (Ln = Ho, Yb) for excellent catalytic performance on cycloaddition reaction of epoxides with CO_2 and Knoevenagel condensation, *ACS Catal.*, 2021, **11**, 14916–14925.
7 T. Sakakura, J.-C. Choi and H. Yasuda, Transformation of carbon dioxide, *Chem. Rev.*, 2007, **107**, 2365–2387.
8 P. Nugent, Y. Belmabkhout, S. D. Burd, A. J. Cairns, R. Luebke, K. Forrest, T. Pham, S. Ma, B. Space, L. Wojtas, M. Eddaoudi and M. J. Zaworotko, Porous materials with optimal adsorption thermodynamics and kinetics for CO_2 separation, *Nature*, 2013, **495**, 80–84.
9 F. Zhang, Y. Wang, X. Zhang, X. Zhang, H. Liu and B. Han, Recent advances in the coupling of CO_2 and epoxides into cyclic carbonates under halogen-free condition, *Green Chem. Eng.*, 2020, **1**, 82–93.
10 X. Huang, X. Gu, H. Zhang, G. Shen, S. Gong, B. Yang, Y. Wang and Y. Chen, Decavanadate-based clusters as bifunctional catalysts for efficient treatment of carbon dioxide and simulant sulfur mustard, *J. CO_2 Util.*, 2021, **45**, 101419.
11 H. Chen, Z. Zhang, T. Hu and X. Zhang, Nanochannel {InZn}–organic framework with a high catalytic performance on CO_2 chemical fixation and deacetalization–Knoevenagel condensation, *Inorg. Chem.*, 2021, **60**, 16429–16438.
12 L. Zhang, S. Yuan, L. Feng, B. Guo, J.-S. Qin, B. Xu, C. Lollar, D. Sun and H.-C. Zhou, Pore-environment engineering with multiple metal sites in rare-earth porphyrinic metal–organic frameworks, *Angew. Chem., Int. Ed.*, 2018, **57**, 5095–5099.
13 V. Guillerm, Ł. J. Weseliński, Y. Belmabkhout, A. Cairns, V. D'Elia, Ł. Wojtas, K. Adil and M. Eddaoudi, Discovery and introduction of a (3,18)-connected net as an ideal

blueprint for the design of metal–organic frameworks, *Nat. Chem.*, 2014, **6**, 673–680.

14 N. Wei, R.-X. Zuo, Y.-Y. Zhang, Z.-B. Han and X.-J. Gu, Robust high-connected rare-earth MOFs as efficient heterogeneous catalysts for CO_2 conversion, *Chem. Commun.*, 2017, **53**, 3224–3227.

15 N. Wei, Y. Zhang, L. Liu, Z.-B. Han and D.-Q. Yuan, Pentanuclear Yb(III) cluster-based metal–organic frameworks as heterogeneous catalysts for CO_2 conversion, *Appl. Catal., B*, 2017, **219**, 603–610.

16 H. Chen, Z. Yang, H. Peng, K. Jie, P. Li, S. Ding, W. Guo, X. Suo, J. Liu, R. Yan, W. Liu, C. L. Do-Thanh, H. Wang, Z. Wang, L. Han, W. Yang and S. Dai, A bifunctional zeolitic porous liquid with incompatible Lewis pairs for antagonistic cascade catalysis, *Chem*, 2021, **7**, 3340–3358.

17 K. C. Nicolaou, D. J. Edmonds and P. G. Bulger, Cascade reactions in total synthesis, *Angew. Chem., Int. Ed.*, 2006, **45**, 7134–7186.

18 K. C. Nicolaou and J. S. Chen, The art of total synthesis through cascade reactions, *Chem. Soc. Rev.*, 2009, **38**, 2993–3009.

19 Z. Jia, K. Wang, B. Tan and Y. Gu, Hollow hyper-cross-linked nanospheres with acid and base sites as efficient and water-stable catalysts for one-pot tandem reactions, *ACS Catal.*, 2017, **7**, 3693–3702.

20 A. Gaona, U. Díaz and A. Corma, Functional acid and base hybrid catalysts organized by associated (organo) aluminosilicate layers for C–C bond forming reactions and tandem processes, *Chem. Mater.*, 2017, **29**, 1599–1612.

21 M. A. Isaacs, C. M. A. Parlett, N. Robinson, L. J. Durndell, J. C. Manayil, S. K. Beaumont, S. Jiang, N. S. Hondow, A. C. Lamb, D. Jampaiah, *et al.*, A spatially orthogonal hierarchically porous acid–base catalyst for cascade and antagonistic reactions, *Nat. Catal.*, 2020, **3**, 921.

22 L.-C. Lee, J. Lu, M. Weck and C. W. Jones, Acid–base bifunctional shell cross-linked micelle nanoreactor for one-pot tandem reaction, *ACS Catal.*, 2016, **6**, 784–787.

23 K. Motokura, M. Tada and Y. Iwasawa, Layered materials with coexisting acidic and basic sites for catalytic one-pot reaction sequences, *J. Am. Chem. Soc.*, 2009, **131**(23), 7944–7945.

24 J. Park, J.-R. Li, Y.-P. Chen, J. Yu, A. A. Yakovenko, Z. U. Wang, L.-B. Sun, P. B. Balbuenab and H.-C. Zhou, A versatile metal–organic framework for carbon dioxide capture and cooperative catalysis, *Chem. Commun.*, 2012, **48**, 9995–9997.

25 B. Li, D. Ma, Y. Li, Y. Zhang, G. Li, Z. Shi, S. Feng, M. J. Zaworotko and S. Ma, Dual functionalized cages in metal–organic frameworks *via* stepwise postsynthetic modification, *Chem. Mater.*, 2016, **28**, 4781–4786.

26 Y. Zhang, Y. Wang, L. Liu, N. Wei, M.-L. Gao, D. Zhao and Z.-B. Han, Robust bifunctional lanthanide cluster based metal–organic frameworks (MOFs) for tandem deacetalization–Knoevenagel reaction, *Inorg. Chem.*, 2018, **57**, 2193–2198.

27 J. Qiao, B. Zhang, X. Yu, X. Zou, X. Liu, L. Zhang and Y. Li, A stable Y(III)-based amide-functionalized metal–organic framework for propane/methane separation and Knoevenagel condensation, *Inorg. Chem.*, 2022, **61**, 3708–3715.

28 P. Wu, J. Wang, Y. Li, C. He, Z. Xie and C. Duan, Luminescent sensing and catalytic performances of a multifunctional lanthanide–organic framework comprising a triphenylamine moiety, *Adv. Funct. Mater.*, 2011, **21**, 2788–2794.

29 C. Yao, S. Zhou, X. Kang, Y. Zhao, R. Yan, Y. Zhang and L. Wen, A cationic Zinc–organic framework with Lewis acidic and basic bifunctional sites as an efficient solvent-free catalyst: CO_2 fixation and Knoevenagel condensation reaction, *Inorg. Chem.*, 2018, **57**(17), 11157–11164.

30 T. Jing, L. Chen, F. Jiang, Y. Yang, K. Zhou, M. Yu, Z. Cao, S. Li and M. Hong, Fabrication of a robust lanthanide metal–organic framework as a multifunctional material for Fe(III) detection, CO_2 capture, and utilization, *Cryst. Growth Des.*, 2018, **18**, 2956–2963.

31 J. Duan, M. Higuchi, R. Krishna, T. Kiyonaga, Y. Tsutsumi, Y. Sato, Y. Kubota, M. Takkata and S. Kitagawa, High $CO_2/N_2/O_2/CO$ separation in a chemically robust porous coordination polymer with low binding energy, *Chem. Sci.*, 2014, **5**, 660–666.

32 R. Zhong, X. Yu and R. Zou, A highly thermal stable microporous lanthanide–organic framework for CO_2 sorption and separation, *Inorg. Chem. Commun.*, 2015, **61**, 17–3176.

33 M. Tian, J. Zheng, J. Xue, X. Pan, D. Zhou, Q. Yao, Y. Li, W. Duan, J. Su and X. Huang, A series of microporous and robust Ln-MOFs showing luminescence properties and catalytic performances towards Knoevenagel reactions, *Dalton Trans.*, 2021, **50**, 17785–17791.

34 Q. Yao, M. Tian, Y. Wang, Y. Meng, J. Wang, Q. Yao, X. Zhou, H. Yang, H. Wang, Y. Li and J. Zhang, A robust, water-stable, and multifunctional praseodymium–organic framework showing permanent porosity, CO_2 adsorption properties, and selective sensing of Fe^{3+} ion, *Chin. J. Struct. Chem.*, 2020, **39**, 1862–1870.

35 Q. Yao, A. B. Gómez, J. Su, V. Pascanu, Y. Yun, H. Zheng, H. Chen, L. Liu, H. N. Abdelhamid, B. Martín-Matute and X. Zou, Series of highly stable isoreticular lanthanide metal–organic frameworks with expanding pore size and tunable luminescent properties, *Chem. Mater.*, 2015, **27**, 5332–5339.

36 Y. Ye, S. Xiong, X. Wu, L. Zhang, Z. Li, L. Wang, X. Ma, Q.-H. Chen, Z. Zhang and S. Xiang, Microporous metal–organic framework stabilized by balanced multiple host-couteranion hydrogen-bonding interactions for high-density CO_2 capture at ambient conditions, *Inorg. Chem.*, 2016, **55**, 292–299.

37 A. M. Bohnsack, I. A. Ibarra, P. W. Hatfield, J. W. Yoon, Y. K. Hwang, J.-S. Chang and S. M. Humphrey, High capacity CO_2 adsorption in a Mg(II)-based phosphine oxide coordination material, *Chem. Commun.*, 2011, **47**, 4899–4901.

38 O. C. Gagné and F. C. Hawthorne, Empirical Lewis acid strengths for 135 cations bonded to oxygen, *Acta Crystallogr.*, 2017, **B73**, 956–961.
39 P. L. Arnold, M. W. McMullon, J. Rieb and F. E. Kühn, C–H bond activation by f-block complexes, *Angew. Chem., Int. Ed.*, 2015, **54**, 82–100.
40 T. Zhang and W. Lin, Metal–organic frameworks for artificial photosynthesis and photocatalysis, *Chem. Soc. Rev.*, 2014, **43**, 5982–5993.
41 M. Almáši, V. Zeleňák, M. Opanasenko and I. Císarová, Ce(III) and Lu(III) metal–organic frameworks with Lewis acid metal sites: preparation, sorption properties and catalytic activity in Knoevenagel condensation, *Catal. Today*, 2015, **243**, 184–194.
42 G. M. Sheldrick, Crystal structure refinement with SHELXL, *Acta Crystallogr.*, 2015, **c71**, 3–8.
43 O. V. Dolomanov, L. J. Bourhis, R. J. Gildea, J. A. K. Howard and H. Puschmann, OLEX2: a complete structure solution, refinement and analysis program, *J. Appl. Crystallogr.*, 2009, **42**, 339–341.